Radiation dose during relativistic electron precipitation events at the International Space Station

H. Ueno[1], S. Nakahira[2], R. Kataoka[3, 4], Y. Asaoka[5], S. Torii[5], S. Ozawa[6], H. Matsumoto[1], A. Bruno[7], G.A. de Nolfo[7], G. Collazuol[8], and S. B. Ricciarini[9]

[1] Research and Development Directorate, Japan Aerospace Exploration Agency, 2-1-1 Sengen, Tsukuba, Ibaraki 305-8505, Japan

[2]High Energy Astrophysics Laboratory, RIKEN, 2-1, Hirosawa, Wako, Saitama 351-0198, Japan

[3]National Institute of Polar Research, 10-3 Midori-cho, Tachikawa, Tokyo 190-8518, Japan.

[4]SOKENDAI, 10-3 Midori-cho, Tachikawa, Tokyo 190-8518, Japan.

[5]Waseda Research Institute for Science and Engineering, Waseda University, 3-4-1 Okubo, Shinjuku, Tokyo 169-8555, Japan

[6]National Institute of Information and Communications Technology (NICT), 4-2-1 Nukui-kitamachi, Koganei, Tokyo 184-8795, Japan.

[7]Heliospheric Physics Laboratory, NASA/GSFC, Greenbelt, MD 20771, USA

[8]Department of Physics and Astronomy, University of Padova, Via Marzolo, 8, 35131 Padova, Italy

[9]Institute of Applied Physics (IFAC), National Research Council (CNR), Via Madonna del Piano, 10, 50019 Sesto, Fiorentino, Italy

Corresponding author: Haruka Ueno (ueno.haruka@jaxa.jp)

Key Points:

- The radiation dose of relativistic electron precipitation (REP) events at the ISS is quantitatively evaluated.
- We have detected 762 REP events during the two and half years observation and the maximum dose per event was 3.0 mSv.
- The radiation dose during a single REP event can exceed the one induced by galactic cosmic rays in one day.

Abstract

We provide a quantitative estimate of the radiation dose during relativistic electron precipitation (REP) events at the International Space Station (ISS). To this goal, we take advantage of the data collected by the CALorimetric Electron Telescope (CALET), the Monitor of All-sky X-ray Image (MAXI), and the Space Environment Data Acquisition equipment – Attached Payload (SEDA-AP). The three ISS detectors offer complementary REP observations, including energy spectra and flux directional information, during a period of approximately two and a half years, from November 2015 to March 2018. We have identified 762 REP events during this period from which we obtain the distribution of radiation dose, relevant to extravehicular activities outside the International Space Station (ISS).

This article has been accepted for publication and undergone full peer review but has not been through the copyediting, typesetting, pagination and proofreading process which may lead to differences between this version and the Version of Record. Please cite this article as doi: 10.1029/2019SW002280

Plain Language Summary

Extravehicular activities outside the International Space Station (ISS) have been exposed to a sporadic radiation dose due to so-called relativistic electron precipitation (REP) events. We evaluate the dose rate of such events at the ISS for the first time to determine whether the dose rate poses a significant danger to the health of astronauts.

1. Introduction

Relativistic electron precipitation (REP) events have been observed for a half century since the findings of unusually enhanced ionization of the mesosphere using radio waves [Bailey and Pomerantz, 1965; Rosenberg et al., 1972]. Direct measurements of REP events, i.e. in-situ observation of MeV electrons, have also been conducted by spacecraft during the last four decades. REP events are a common feature near the radiation belt, as measured by several spacecraft (Anderson et al., 1968; Imhof et al., 1986; Lorentzen et al., 2000; Carson et al., 2013; Comess, et al., 2013).

Recently, REP events have been considered one of the fundamental loss processes of outer radiation belt electrons (Millan et al., 2002; Lorentzen et al. 2000; Kubota et al. 2015; Kurita et al., 2018). A basic understanding of REP events thus contributes to predicting the dynamic variation of the radiation belts, which is a major target of space weather forecasts. REP events may also play a possible role in linking space and climate, as energetic electrons ionize Earth's middle atmosphere to create nitrogen oxides that act as a catalyst to destroy ozone (Daae et al., 2012; Isono et al., 2014a; 2014b). It is therefore important to quantify the total amount of radiation associated with REP events. In this paper we do so in the context of radiation dose to humans who may participate in extravehicular activities at the International Space Station.

Kataoka et al. (2016) have reported the detection of REP events at the International Space Station (ISS) with the Charge Detector (CHD) onboard the CALorimetric Electron Telescope (CALET; Torii et al., 2017). As a result, a newly raised important aspect of REP events concerns the radiation exposure for astronauts, especially during extravehicular activities (EVA). The bottom layer of the space suit helmet is called a protective visor which is made of polycarbonate with a thickness of about 0.2 g/cm^2 (Wilson et al. 1997). The upper layer is equipped with a sun visor to shield the sunlight. In order to estimate the maximum exposure in the EVA, we assumed that it is protected with a protective visor. The electron energy of >0.5 MeV is required to penetrate through a polycarbonate with a thickness of 0.2 g/cm^2 (Berger et al. 1998), and needed to be considered in the dose rate estimate. However, a quantitative analysis of radiation dose cannot be made by the CALET alone because real-time data only give the integrated counts of MeV electrons every second without detailed information about the energy spectra.

The Standard DOse Monitor (SDOM) is one of the sensors installed on the Space Environment Data Acquisition equipment – Attached Payload (SEDA-AP), which is also onboard the ISS (Matsumoto et al., 2001). The SDOM was designed for dose assessment , and can measure energy spectra of energetic electrons every 10 seconds.

The Monitor of All-sky X-ray Image (MAXI) includes the Radiation Belt Monitor (RBM), which is another useful sensor for investigating REP events. It can play a similar role with the CHD to monitor energetic electrons at one-second time cadence in two perpendicular directions (i.e., both horizontal and vertical directions) at an energy range starting from 300 keV. The RBM data therefore gives some information on the pitch angle distribution of REP events at low energy. As the CHD is pointed toward the zenith direction and the SDOM is pointed toward the horizontal direction, the RBM indirectly helps to compare these two data

sets. It is thus possible to characterize the REP events complementarily by combining the data obtained from the CHD, RBM and SDOM.

The purpose of this study is to evaluate the actual dose rate during a 2.5 year time period when data from all the instruments was available. This paper describes the first such attempt based on the complementary use of these three independent instruments. Section 2 explains the basic configurations of each instrument. Section 3 describes the method of detecting REP events. In Section 4, we discuss the radiation dose rate of REP events quantitatively. Concluding remarks are summarized in Section 5.

2. Instruments and Data

The three detectors used in this work (CHD, RMB and SDOM) were located on the same exposure module of the ISS, as shown in Figure 1. The analyzed data sample is limited to the time interval of approximately two and a half years (November 2015 – March 2018) when the three instruments were operative. The SEDA-AP completed its operation in March 2018, the CALET began observation in October 2015, and the MAXI has continued observation since August 2009. Table 1 lists the energy ranges of the SDOM, CHD, and RBM.

CALET has been measuring GeV-TeV electrons and nuclei in Z = 1-40 and gamma ray bursts since October 2015 (Asaoka et al., 2018). The high count rate of the CHD is monitored as "bad space weather," especially in high-latitude paths to carefully operate the high-voltage system of the CALET. The CHD is placed on top of the apparatus to measure the electric charge of incoming particles via the Z^2 dependence of the specific ionization loss in the double layered, segmented, plastic scintillator array. Each layer consists of 14 plastic scintillator paddles, with dimensions 450 mm (L) × 32 mm (W) × 10 mm (H). The two layers of paddles (i.e., CHD-X and CHD-Y) are orthogonally arranged to determine the incident position of cosmic rays. The CHD and related front-end electronics are designed to provide incident particle identification with sufficient charge resolution over a large dynamic range for charges from Z = 1 to Z = 40 (Akaike et al., 2019). The analog sum of signals in each CHD layer feeds a discriminator with an approximate 0.6 MeV threshold to produce a trigger counter signal. Coincidence between the signals including those from other detector components produces the event trigger for cosmic rays (Asaoka et al., 2018). The trigger counter signals are counted with a scalar, and the numbers per second are recorded as part of the housekeeping data. These signals are used in this analysis to obtain the count rates of the CHD-X and the CHD-Y, and the ratio r_{XY}.

The SDOM has been measuring the energy spectra for electrons of 0.28—20.01 MeV and protons of 1-250 MeV that has been operated since August 2009 (Matsumoto et al., 2001). The line of sight of the SDOM was changed from the zenith direction to the horizontal direction after the relocation of SEDA-AP in August 2015. The SDOM contributes to dose assessment of the ISS mission and the evaluation of space radiation models in the low Earth orbit environment. The SDOM consists of three silicon detectors, a plastic scintillator with two photo-multiplier tubes, and an anticoincidence scintillator. The thicknesses of the three silicon detectors and the plastic scintillator are 134 μm, 300 μm, 1000 μm, and 56 mm, respectively. A 12.7 μm-thick kapton window prevents the detection of low-energy particles and photons. The combination of deposited energies in each sensor is used to derive the incident particle atomic number and energy. The SDOM measures the energy spectra of electrons at seven energy channels ranging from 0.28 to 20.01 MeV. The fluxes of each energy channels were calculated from following equation;

$$N_i = t_{\text{sample}} F\left(E_{\text{avg}}\right) G_i \, \text{FWHM}_i, \quad (1)$$

where t_{sample} is the sample time, $F(E_{\text{avg}})$ is the omnidirectional flux at the average bin energy, G_i is the weighted average geometric factor, and $FWHM_i$,is the full-width half-maximum energy of the ith energy channel. The sample time of SDOM was set to 10 seconds. Table 2 summarizes the calibration constants. The geometric factors were calculated from combined the result of the Monte Carlo simulations based on the CERN-GEANT code (Burn et al., 1994) and the detection pattern of each energy channel. The two highest energy channels, CH6 and CH7, are affected by contamination from high-energy cosmic-ray protons and electrons; however, these channels were not considered in the analysis presented in this paper.

The RBM is a support sensor of the MAXI (Matsuoka et al., 2009), which is intended to protect the Gas-Slit camera consisting of proportional counters operating at high voltage (1550-1650 V) against heavy irradiation. If the count rate registered by the RBM exceeds a given threshold, high voltages are automatically reset to 0 V. The high voltages are automatically recovered when the RBM count rate becomes lower than the 50% of the threshold level. The RBM consists of two units of PIN diode detectors that face the horizontal and zenith directions. Having a detection area of 5×5 mm^2 and 200 μm thickness with an optical blocking filter of 50 μm aluminum, the RBM is sensitive to electrons above 0.3 MeV and protons above 3 MeV. The particle trigger counts are accumulated on a one-second basis up to about 10^5 counts s^{-1}.

3. Methods

The identification of REP events is based on the combined data from the RBM and the CHD. Because of the lower energy threshold of RBM, the selected sample also comprises weaker amplitude REP-like events with respect to the simple threshold classification by Kataoka et al. (2016). First, we detect rough candidate 60-second time intervals of a rapid variation when the derivative count rate of the RBM-Z exceeds 500 counts s^{-2}. Then in selecting "most likely" REP events, we employed the intensity ratio r_{XY}. When r_{XY} is much greater than 1.0 it can be a result of a very efficient MeV electron precipitation (Kataoka et al. 2016). Therefore, when r_{XY} is statistically greater than 1.0 by 3-sigma, we identified the time interval as a REP event. In this study we excluded the events detected in the South Atlantic Anomaly and their vicinity by not including longitudes between 90 and 200 degrees with latitude below 0 degree.

We detected 762 "most likely" REP events in total during the two and a half years from 1 November 2015 to March 31 2018. We confirmed that the REP events identified using the above method include all of the REP events as documented by Kataoka et al. (2016). Figure 2 shows two examples of a REP event occurring around (a) 14:47 UT on 4 November 2015 and (b) 13:01UT on 9 March. List and plots of all the REP events extracted in this research can be checked at our web page (http://darts.isas.jaxa.jp/pub/maxi/rbm/references/ueno2019spw/).

We then evaluate the exposure dose through the helmet visor when an astronaut encounters a REP event during EVA. It is assumed that the incident flux coincides with the one measured by SDOM. The effective dose rate (D), assuming that the REP-derived electron beam comes from the 4π direction, is calculated by the following equation:

$$D = \sum_{i=1,\cdots,5} 4\pi C_i F_i \delta E_i \qquad (2)$$

where *i* denotes the energy channel, and *F* is the flux at corresponding energy bin widthδE. The flux-to-dose conversion coefficient was calculated by extrapolating the conversion coefficient at the center value of each energy channel of SDOM from the recommended value of ICRP116 (an isotropic case). The central value at CH1 is 0.5 MeV, and it is reasonable to estimate that

an electron beam above the lowest energy channel of SDOM can penetrate the helmet visor of the space suit. Table 3 lists the flux-to-dose conversion coefficients and the width of energy bin in each energy channel.From this table, it can be seen that the electrons with larger energy give more affect to the lens of eye. Then the radiation dose for each REP event was calculated by integrating the equation with SDOM data collected every ten seconds over the REP time intervals defined based on CHD data. We also assume that detailed corrections beyond the descriptions of Matsumoto et al. (2001), such as the aging effect, are negligible in roughly evaluating possible maximum values. Note that the largest uncertainties in this study come from the assumption of isotropic precipitation, and it always gives the overestimate by roughly a factor of 2 if not isotropic.

4. Results and Discussion

Figure 3 (a) shows the distribution of the event duration and effective dose rate of the REP events, detected from November 2015 to March 2018. The geographical distribution of the REP events is shown in Figure 3 (b). It is evident that the REP events occured at high geographic latitude and high geomagnetic latitude regions. We employed SDOM data for the dose calculation using five energy bins. Due to operational constraints on thermal condition of SDOM, its detection efficiency was limited to 55%. Thus, we used 362 events observed with SDOM out of total 762 REP events. The dose is found to be roughly proportional to event duration, having broad peaks around 0.1-1 mSv per event and durations of 200-600 seconds. They typically show double peaked time series in CHD, as shown in Figure 2(a). Note that the REP phenomena themselves can be long-lived (e.g., Blake et al., 1996) and the ISS orbit samples across the phenomena for a short time. We obtain the integrated dose of REP events to be 123.1 mSv in 881 days. By correcting for SDOM efficiency, the averaged dose rate becomes 92 mSv/year. We have detected 34 events which exceed 1 mSv/event, with the maximum of 3.0 mSv/event. The dose rate of REP events is higher than the other factors such as galactic cosmic rays, solar energetic particles, and radiation belt particles at South Atlantic Anomaly (Dachev et al., 2017), although the duration is short.

Note that solar activity in this time period was in a declining phase when the radiation belts were relatively active. A number of moderate magnetic storms occurred, mainly caused by high-speed solar wind streams from coronal holes (e.g., Kataoka and Miyoshi, 2006; Kataoka and Miyoshi, 2009; Turner et al., 2019). The two and a half year statistics thus provide the data for relatively active radiation belts, although a longer-term study is warranted to determine the range of expected dose rates. A follow-up study is also needed to determine the relation to geomagnetic activity levels.

It is noteworthy that the present study estimated the REP-associated dose rate for EVA activity outside of ISS, and the maximum dose rate of 3 mSv per event, which exceeds the daily averaged dose rate at ISS. Although NCRP recommends reducing the occupational exposure limit of the lens of eye from 150 mGy to 50 mGy (Dauer et al.,2017), this result revealed that the exposure dose of the lens of eye by REP events is lower than the recommended limit. Since similar REP events tend to persist from orbit to orbit for several hours, possibly associated with substorm activities or magnetic storms, the total radiation dose during an EVA becomes a few to ten mSv in the worst case. Consequently, while the relative contribution to the cumulative radiation exposure over long periods of several months is not relevant compared to other components, e.g. 1.1 mSv/day estimated for Galactic cosmic-rays at solar minimum (Sato et al., 2017), the dose associated with REP intervals can be significant over a few hour timescale of typical EVA.

5. Conclusion

We have evaluated REP contribution to the radiation for astronauts during the EVA. We have identified REP events with CHD and RBM data, and determined the radiation dose for each event from SDOM data. During a two and a half year period, 762 REPs were detected, with 34 relatively strong REP events exceeding 1 mSv/event per event including the largest event of 3 mSv per event. Such low values will not affect the astronauts' health. We anticipate that the list of REP events provided in this paper will help to form future collaborative studies.

Acknowledgments

This research made use of MAXI/RBM data provided by RIKEN, JAXA, and the MAXI team, which is available via DARTS. The CALET/CHD data used in this analysis were provided by the Waseda CALET Operation Center at Waseda University. The DARTS website of JAXA provides the MAXI/RBM (http://darts.isas.jaxa.jp/pub/maxi/rbm/) and CALET/CHD (http://darts.isas.jaxa.jp/pub/calet/cal-v1.0/CHD/level1.1/). The Space Environment & Effects System of JAXA provided spectra data from the SEDA-AP/SDOM (http://seesproxy.tksc.jaxa.jp/fw/dfw/SEES/English/Top/top_e.shtml). RK is funded by JSPS KAKENHI 17K05671. YA and RK are supported by JSPS KAKENHI 17H02901.

References

Akaike, Y. for the CALET Collaboration (2019), Measurements of Heavy Cosmic-Ray Nuclei Spectra with CALET on the ISS, Journal of Physics: Conference Series, 1181, 1, 012042

Anderson, H. R., Hudson, P. D., and McCoy, J. E. (1968), Observations of POGO ion chamber experiment in the outer radiation zone, *J. Geophys. Res.*, 73, 6285-6297.

Asaoka, Y., Ozawa, S., Torii, S. et al. (CALET collaboration) (2018), On-orbit operations and offline data processing of CALET onboard the ISS. *Astroparticle Physics*, 100, 29-37.

Bailey, D. K., and Pomerantz, M. A. (1965), Relativistic electron precipitation into the mesosphere at subauroral latitudes, *J. Geophys. Res.*, 70, 5823-5830.

Berger, M. J., J. S. Coursey, M. A. Zucker, and J. Chang (2011), Stopping-power and range tables for electrons, protons, and helium ions, NIST, Physical Measurement Laboratory, Gaithersburg, Md. [Available at http://www.nist.gov/pml/data/star.]

Blake, J. B., M. D. Looper, D. N. Baker, R. Nakamura, B. Klecker, and D. Hovestadt (1996), New high temporal and spatial resolution measurements by SAMPEX of the precipitation of relativistic electrons, Adv. Space Res., 18(8), 171-186.

Brun, R., et al. (1994), GEANT detector description and simulation tool, *W5014*, Comput. and Networks Div., Eur. Org. for Nucl. Res., Geneva, Switzerland.

Carson, B. R., C. J. Rodger, and M. A. Clilverd (2013), POES satel-lite observations of EMIC-wave driven relativistic electron precipita-tion during 1998-2010, *J. Geophys. Res. Space Physics,*118, 232–243,doi:10.1029/2012JA017998.

Comess, M. D., D. M. Smith, R. S. Selesnick, R. M. Millan, and J. G. Sample (2013), Duskside relativistic electron precipitation as measuredby SAMPEX: A statistical survey, *J. Geophys. Res. Space Physics*, 118, 5050–5058, doi:10.1002/jgra.50481.

Daae, M., Espy, P., H. Nesse Tyssoy, Newnham, D., Stadsnes, J. & Soraas, F. (2012), The effect of energetic electron precipitation on middle mesospheric night-time ozone during and after a moderate geomagnetic storm. *Geophysical Research Letters*, 39, L21811, http://doi.org/doi:10.1029/2012GL053787.

Dachev, T. P., Bankov, N. G., Tomov, B. T., Matviichuk, Y. N., Dimitrov, P. G., Hader, D.-P., & Horneck, G. (2017). Overview of the ISS radiation environment observed during the ESA EXPOSE-R2 mission in 2014-2016. *Space Weather*, 15, 1475-1489. https://doi.org/10.1002/2016SW001580.

Dauer, L.T., et al. (2017), Guidance on radiation dose limits for the lens of the eye: overview of the recommendations in NCRP Commentary No. 26, *Int J Radiat Biol.*, 93(10), 1015-1023. https://doi.org/10.1080/09553002.2017.1304669.

ICRP (2010), Conversion Coefficients for Radiological Protection Quantities for External Radiation Exposures, ICRP Publication 116, Ann. ICRP 40, 2–5.

Imhof, W. L., Voss, H. D., Reagan, J. B., Datlowe, D. W., Gaines, E. E., Mobilia, J., and Evans, D. S. (1986), Relativistic electron and energetic ion precipitation spikes near the plasmapause, *J. Geophys. Res.*, 91, 3077-3088.

Isono, Y., Mizuno, A., Nagahama, T., Miyoshi, Y., Nakamura, T., Kataoka, R., Tsutsumi, M., Ejiri, K., Fujiwara, H., Maezawa, H. & Uemura, M. (2014), Ground-based observations of nitric oxide in the mesosphere and lower thermosphere over Antarctica in 2012-2013, *J. Geophys. Res.: Space Physics*, 119(9), 7745.

Isono, Y., Mizuno, A., Nagahama, T., Miyoshi, Y., Nakamura, T., Kataoka, R., Tsutsumi, M., Ejiri, K., Fujiwara, H., & Maezawa, H. (2014), Variations of nitric oxide in the mesosphere and lower thermosphere over Antarctica associated with a magnetic storm in April 2012, *Geophysical Research Letters*, 41(7), 2568.

Kataoka, R., Asaoka, Y., Torii, S., Terasawa, T., Ozawa, S., Tamura, T., Shimizu, Y., Akaike, Y., & Mori, M. (2016), Relativistic electron precipitation at International Space Station: Space weather monitoring by Calorimetric Electron Telescope. *Geophysical Research Letters*, 43, 4119-4125, http://doi.org/doi:10.1002/2016GL068930.

Kataoka, R., and Miyoshi, Y. (2006), Flux enhancement of radiation belt electrons during geomagnetic storms driven by coronal mass ejections and corotating interaction regions, *Space Weather*, 4(9).

Kataoka, R., and Y. Miyoshi (2010), Why are relativistic electrons persistently quiet at geosynchronous orbit in 2009?, *Space Weather*, 8, S08002, doi:10.1029/2010SW000571.

Kubota, Y., Omura, Y., and Summers, D. (2015), Relativistic electron precipitation induced by EMIC-triggered emissions in a dipole magnetosphere, *J. Geophys. Res. Space Physics*, 120, 4384, 4399, doi:10.1002/2015JA021017.

Kurita, S., Miyoshi, Y., Shiokawa, K., Higashio, N., Mitani, T., Takashima, T., et al. (2018). Rapid loss of relativistic electrons by EMIC waves in the outer radiation belt observed by Arase, Van Allen Probes, and the PWING ground stations, *Geophysical Research Letters*, 45, 12,720-12,729. https://doi.org/10.1029/2018GL080262.

Li, W., Ni, B., Thorne, R. M., Bortnik, J., Green, J. C., Kletzing, C. A., Kurth, W. S., and Hospodarsky, G. B. (2013), Constructing the global distribution of chorus wave

intensity using measurements of electrons by the POES satellites and waves by the Van Allen Probes, Geophys. Res. Lett., 40, 4526-4532, doi:10.1002/grl.50920.

Lorentzen, K. R., McCarthy, M. P., Parks, G. K., Foat, J. E., Millan, R. M., Smith, D. M., Lin, R. P. & Treilhou J. P. (2000), Precipitation of relativistic electrons by interaction with electromagnetic ion cyclotron waves, *Geophysical Research Letters*, 105, 5381–5389.

Matsumoto, H., Koshiishi, H., Goka, T., Kimoto, Y., Green, B. D., Galica, G. E., Nakamura, T., Abe, T., Badono, S., Murata, S., & Sullivan, J. D. (2001), Compact, lightweight spectrometer for energetic particles, *IEEE Transactions on Nuclear Science*, 48(6), 2043-2049.

Matsuoka, M., et al. (2009), The MAXI mission on the ISS: Science and instruments for monitoring All-sky X-ray Images, *Publications of the Astronomical Society of Japan*, 61(5), 999-1010.

Millan, R. M., R. P. Lin, D. M. Smith, K. R. Lorentzen (2002), and M. P. McCarthy, X-ray observations of MeV electron precipitation with a balloon-borne germanium spectrometer, *Geophys. Res. Lett.*, 29(24), 2194, doi: 10.1029/2002GL015922.

Petoussi-Henss, N., et al. (2010), Conversion coefficients for radiological protection quantities for external radiation exposures. *Annals of the ICRP*, 40(2), 1-257.

Rosenberg, T. J., Lanzerotti, L. J., Bailey, D. K., and Pierson, J. D. (1972), Energy spectra in relativistic electron precipitation events, *J. Atmos. Terr. Phys.*, 34, 1977-1989.

Sato, T., Nagamatsu, A., Ueno, H., Kataoka, R., Miyake, S., Takeda, K., Niita, K. (2017), Comparison of Cosmic-Ray Environments on Earth, Moon, Mars and in Spacecraft Using PHITS, *Radiat. Prot. Dosim.*, doi:10.1093/rpd/ncx192.

Torii, S., et al. (2017), The CALorimetric Electron Telescope (CALET) on the ISS: Preliminary Results from On-orbit Observations since October, 2015, in *Proceeding of Science* (ICRC2017), 1092.

Turner, D. L., Kilpua, E. K. J., Hietala, H., Claudepierre, S. G., O'Brien, T. P., Fennell, J. F., et al. (2019). The response of Earth's electron radiation belts to geomagnetic storms: Statistics from the Van Allen Probes era including effects from different storm drivers. Journal of Geophysical Research: Space Physics, 124, 1013-1034. https://doi.org/10.1029/2018JA026066

Wilson, J. W., Miller, J., Konradi, A., and Cucinotta, F. A. (1997), Shielding strategies for human space exploration, *NASA Conference Publications* 3360, edited by J. W. Wilson, J. Miller, A. Konradi, and F. A. Cucinotta.

Table 1. Energy range of electrons as observed by SDOM, CHD, and RBM

Instruments	Energy range of electrons [MeV]	Time resolution [sec]
SEDA-AP/SDOM CH1	0.28-0.79	
SEDA-AP/SDOM CH2	0.93-1.85	
SEDA-AP/SDOM CH3	1.58-3.44	
SEDA-AP/SDOM CH4	3.30-5.50	10
SEDA-AP/SDOM CH5	5.31-10.23	
SEDA-AP/SDOM CH6	8.27-18.10	
SEDA-AP/SDOM CH7	13.16-21.01	
CALET/CHD X	> 1.6	1
CALET/CHD Y	> 3.6	
MAXI/RBM	> 0.3	1

Table 2. Calibration constants in the electron measurements for SEDA-AP/SDOM

Energy channels	G_i [cm^2 sr]	FWHM$_i$ [MeV]
CH1	0.093	0.50
CH2	0.046	0.92
CH3	0.036	1.94
CH4	0.103	2.23
CH5	0.124	5.26

Table 3. Flux-to-dose conversion coefficients in each energy channels

Energy channels	Energy bin width [MeV]	Flux-to-dose conversion coefficients [pGy cm^2]
CH1	0.50	0.03
CH2	0.92	40.54
CH3	1.94	88.34
CH4	2.23	117.75
CH5	5.26	146.70

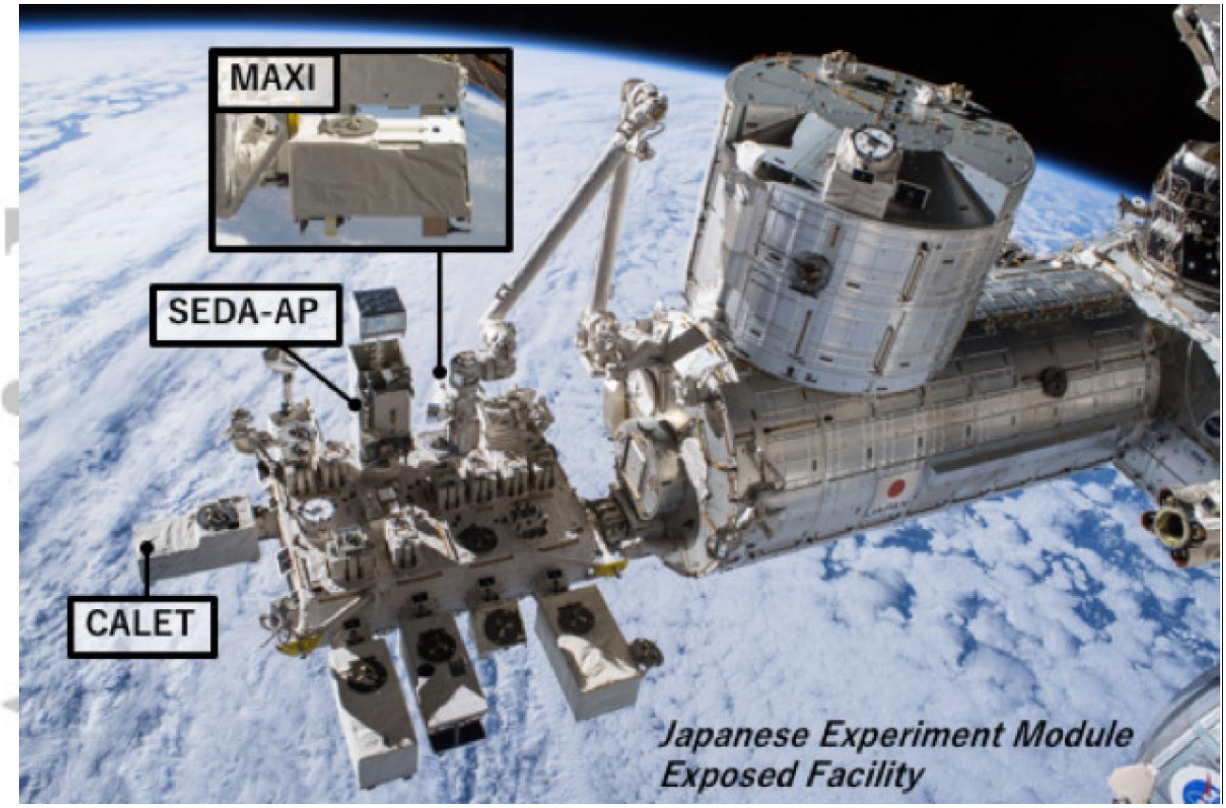

Figure 1. Locations of CALET/CHD, MAXI/RBM, and SEDA-AP/SDOM on the exposure module of ISS (credit: JAXA/NASA)

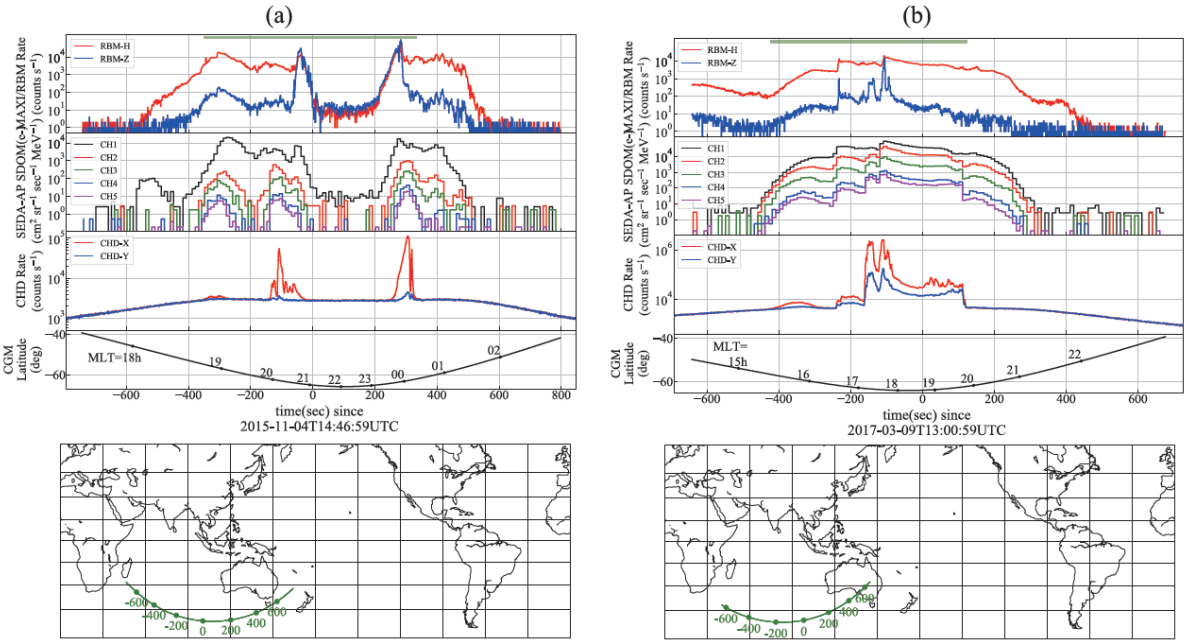

Figure 2. The time series of all sensors (top three panels) and geographic location of a REP event (bottom panel); (a) 14:47 UT on 4 November 2015 and (b) 13:01 UT on 9 March. The green horizontal bar in the top panel shows the time interval used in the dose calculation for a REP event.

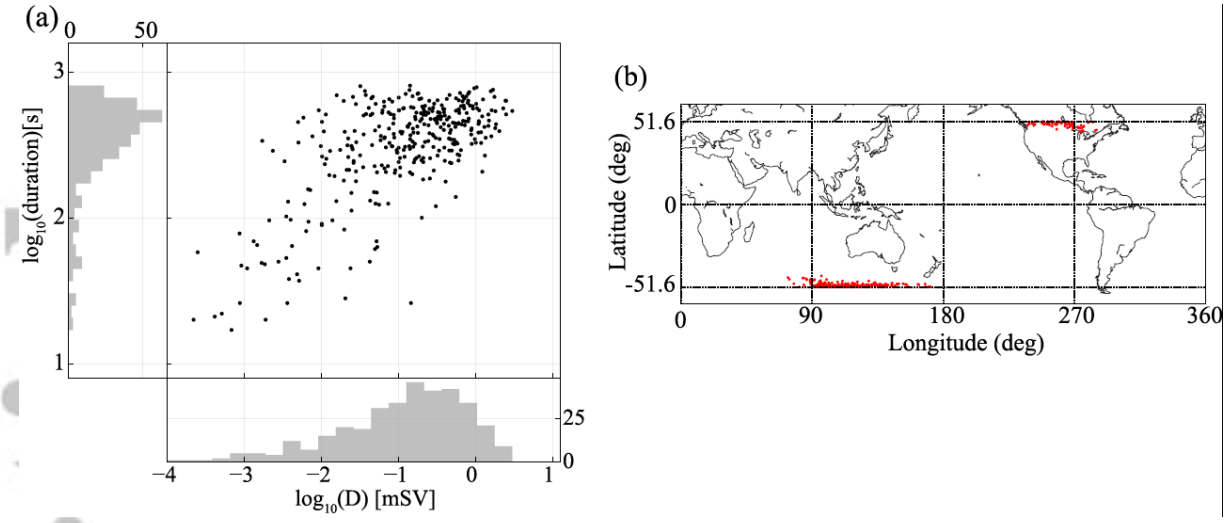

Figure 3. (a) The histogram of REP event duration versus dose and their projections. (b) The distribution of REP events in the geographic coordinate system.